ACS APPLIED ENERGY MATERIALS

www.acsaem.org Article

Performance Analysis and Optimization of a SnSe-Based Thermoelectric Generator

Monikuntala Bhattacharya, Mani Ranjan, Nitish Kumar, and Tanmoy Maiti*

Cite This: *ACS Appl. Energy Mater.* 2021, 4, 8211−8219 Read Online

ACCESS | Metrics & More | Article Recommendations | Supporting Information

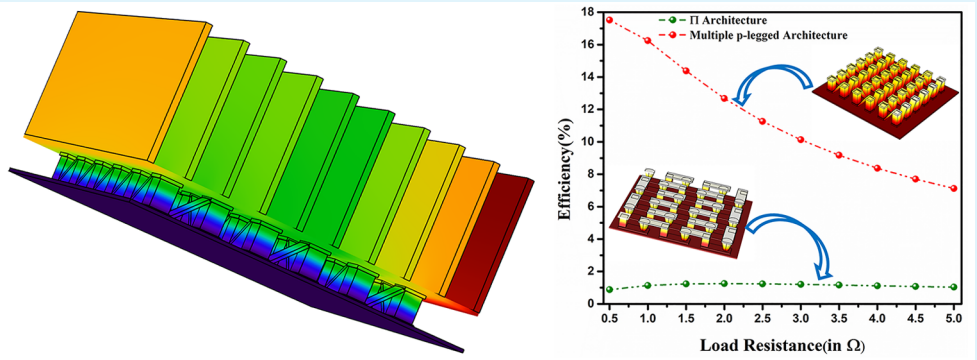

ABSTRACT: The thermoelectric generator (TEG) is considered as one of the most promising technologies for clean energy generation. But performance optimization with respect to its design and architecture is required for wide-scale commercialization. In this study, we have carried out finite element modeling (FEM) of a SnSe-based thermoelectric generator (TEG) considering electrical contact loss and various heat losses under isothermal and isoflux heat boundary conditions. The conventional Π-architecture comprising both p- and n-legs often results in overall poor performance due to the inferior efficiency of the n-leg TE module compared to its p-counterpart even though SnSe holds high *ZT* values (≥2). To counter that, we have strategized to design only a p-legged architecture and evaluated its performance in terms of power output and efficiency. Step-by-step optimization of internal and system level parameters for a multiple p-legged as well as traditional p−n-legged TEG has been carried out. Further, Al-based fins have been used to increase the net heat capturing area in the case of the isoflux heat boundary condition. The incorporation of fins facilitates us to redefine an internal parameter called fill fraction (*FF*) in terms of system level parameters, which leads to easier optimization of the TEG. Keeping in mind the practical application of a TEG in automobile exhaust, simulation of multiple p-legged architecture has resulted in maximum power output of 6.61 and 3.45 W under the isothermal and isoflux heat boundary conditions, respectively. In the FEM considering various thermal and electrical losses under the isothermal heat boundary condition, a maximum efficiency of 4.8% has been obtained in the case of Π-architecture, which is slightly higher than that obtained in the multiple p-legged TEG (3.48%). However, under the isoflux scenario, which is more commonly found in practical waste-heat sources, a maximum efficiency of 17.5% has been achieved for multiple p-legged architecture, which is 14 times higher than that attained for Π-architecture (1.24%). Also, a huge surge (500%) in maximum power output has been observed for the proposed multiple p-legged TEG compared to Π-architecture in our FEM considering various thermal and electrical losses in the isoflux heat source condition. Furthermore, the investigation of thermal and mechanical stability in terms of generated von Mises stress and deformation due to a significant temperature difference has revealed that multiple p-legged architecture is indeed more stable as compared to a Π-architecture TEG under both of the heat boundary conditions.

KEYWORDS: *thermoelectric generator (TEG), fill fraction (FF), isoflux condition, unileg, finite element modeling, automotive exhaust*

INTRODUCTION

Global warming due to the excessive use of fossil fuel is one of the biggest concerns of today's world, which has compelled the scientific community to look for alternative green energy resources. A recent study has divulged that effectively 72% of global primary energy gets wasted as heat.[1] In diesel engines, only 30−40% of chemical energy can be converted into mechanical energy,[2] from which only one-third can be utilized for propulsion, and the rest comes out as heat through

Received: May 24, 2021
Accepted: July 12, 2021
Published: July 22, 2021

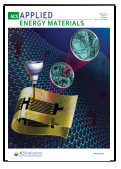

https://doi.org/10.1021/acsaem.1c01466
ACS Appl. Energy Mater. 2021, 4, 8211−8219

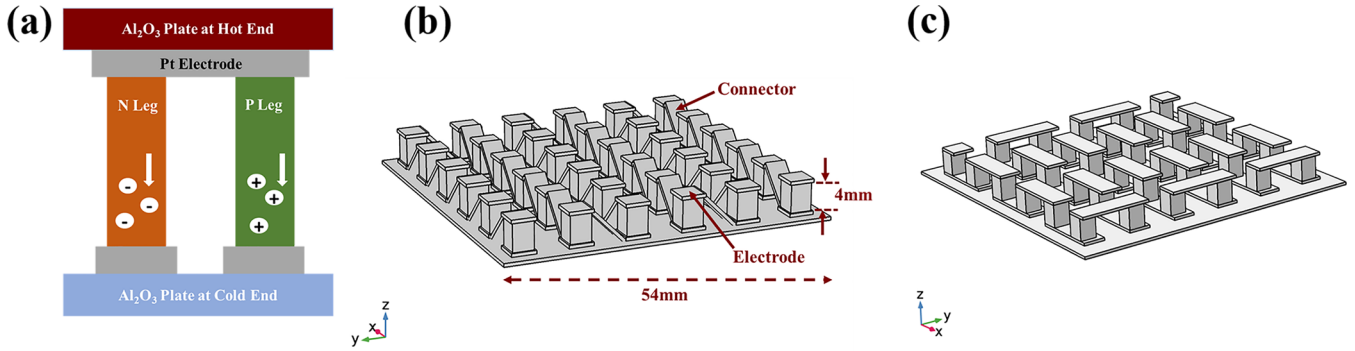

Figure 1. (a) Schematic diagram of unicouple model. (b) Multiple p-legged and (c) multiple p−n-legged TEG.

exhaust.[3] Recovery of waste heat using a solid state thermoelectric generator (TEG) can be a feasible alternative, in which waste thermal energy gets directly converted into electrical energy using the Seebeck effect. Moreover, the absence of moving parts in the TEG ensures compact, reliable, and quiet operation,[4] making it attractive for application in small-scale power generation.[5] A TEG is generally comprised of p- and n-type thermoelectric legs (Figure 1a), connected in such a way that an electrical series connection and thermal parallel connection can be formed. The potential of thermoelectric materials to efficiently produce power can be determined by the figure of merit, $(ZT) = \frac{S^2\sigma}{K_l + K_e}T$, where S, σ, K_l, K_e, and T are the Seebeck coefficient, electrical conductivity, lattice thermal conductivity, electronic thermal conductivity of the material, and absolute temperature, respectively.[6] State-of-the-art thermoelectric materials such as selenides and tellurides demonstrate satisfactorily high ZT (∼2) values[7] at low and midtemperature regions (∼700−800 K). Despite high ZT values, the typical energy conversion efficiency of commercially available TEGs is ∼5−7%,[8] which is very inferior compared to the other renewable energy sources, e.g., it is more than 25% for the solar cell.[9,10] As a result, the widescale commercialization of the TEG has not been implemented until today. To improve the efficiency of the TEG, it is of utmost necessity to address the associated thermal and electrical losses, which are significantly impacted by various device parameters. Optimization of device parameters in terms of internal parameters[11−15] such as leg spacing, leg geometry, number of leg pairs, as well as dimensionless parameters such as the fill fraction,[16] aspect ratio,[17] and other shape factors[18] for system level optimization[19,20] can potentially enhance the electrical performance of the TEG using available TE materials.

However, optimization of all these parameters requires thousands of experimental trials, which is quite time-consuming and almost impossible for product development in terms of investment cost. Performance optimization using device simulation can be a suitable alternative to determine these variable parameters in order to achieve maximum power output and energy conversion efficiency. Solving various thermoelectric effects,[21] namely, the Seebeck effect, Peltier effect, and Thomson effect, on discretized finite elements of a TE leg geometry and calculating the overall power generation can provide a better estimation of the energy conversion efficiency of a thermoelectric module. A few fruitful reports[22−24] on design and performance optimization of the TEG using finite element modeling (FEM) by ANSYS or COMSOL Multiphysics software have been published in the recent years.

Moreover, continuous thermal cycling and an elevated temperature difference generate thermal stress into the TEG module, which affects the thermoelectric performance[24] and may eventually lead to structural and mechanical failures.[25] The device element cross-sectional area,[26] mismatch of the coefficient of thermal expansion (CTE),[27] and device geometry[28] influence the thermomechanical stability as well as the lifetime of the TEG. A comprehensive study on the impact of geometrical parameters on thermal stress has shown that a thinner alumina plate as a heat collector (thickness ≤ 2.5 mm) and a smaller gap between thermoelectric legs can efficiently reduce the thermal stress generated in a Bi_2Te_3-based TEG.[24]

Although studies on the optimization of a conventional (p−n) Π-TEG and a few unilegged architectures[29−31] are available in the literature, most of them have dealt with the isothermal heat boundary condition,[32] where the hot end temperature remains fixed. However, in practical scenarios, most of the heat sources (such as automotive exhaust, industrial flue gas, etc.) impart heat at a constant rate, i.e., constant heat flux, also termed as isoflux heat boundaries,[33] resulting in an inferior performance of the TEG in a real-world application.

In the present work, finite element modeling of the multiple p-legged TEG has been established. Its electrical performance has been studied under the isothermal as well as isoflux heat boundary condition using COMSOL Multiphysics, aiming for its application in automobile exhaust. The maximum temperature in the exhaust of a diesel-powered automobile vehicle can reach up to 773 K,[34] which requires TE material having good thermal stability along with high ZT values. Here, we have considered doped SnSe as a suitable TE material for such a kind of application, since it exhibits high ZT values (>2)[35−38] in the form of both n-type and p-type material.

In the present work, we have shown that the proper geometrical optimization and enhancement of the heat capturing area under the isoflux heat boundary condition can lead to the striking enhancement of maximum power output for the multiple p-legged TEG by 500% compared to the optimized multiple p−n-legged (Π) architecture. In that context, a relationship between internal parameters and system level parameters has been established to redefine the fill fraction (FF) for the isoflux heat boundary condition. Furthermore, the detailed thermal stress analysis has been carried out in terms of von Mises stress generation and deformation due to generated stress for both the isothermal and isoflux heat boundary conditions, taking into account the

https://doi.org/10.1021/acsaem.1c01466
ACS Appl. Energy Mater. 2021, 4, 8211−8219

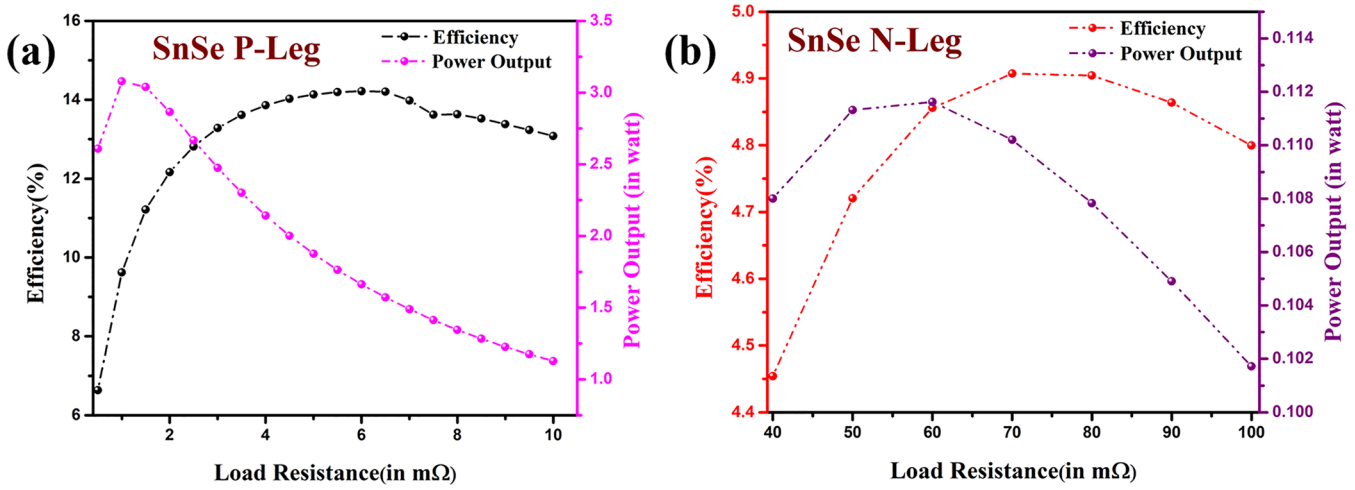

Figure 2. Power output and efficiency vs load resistance for (a) single p and (b) single n thermoelectric leg.

high temperature difference and high input heat flux. The investigation has shown that the generation of stress and deformation is much less for the multiple p-legged architecture than Π-architecture TEG.

METHODOLOGY

Thermoelectric Generator Model. Utilizing finite element modeling (FEM) in COMSOL Multiphysics, 36 p-type SnSe legs have been placed in between two 5.4 × 5.4 cm ceramic (Al_2O_3) substrates at a fixed leg spacing of 5 mm. The legs are connected electrically in series and thermally in parallel via platinum (Pt) connectors and electrodes, as shown in Figure 1(b). The outer surfaces of Al_2O_3 substrates have been considered as the thermal boundary for simulation. A constant heat flux of ~10^4 W/m^2 (observed between the takedown inlet and tailpipe exit of the automobile exhaust[39]) under the isoflux condition and a fixed temperature of T_h = 773 K under the isothermal condition have been applied at the hot side of the module. Further, the optimized 36 p−n-multilegged TEG (Figure 1(c)) has been simulated in order to compare its performance with the p-legged TEG. The thermoelectric properties used for simulation of n-[36] and p-type[38] SnSe legs are shown in Figure S1. In order to enlarge the heat capturing area under the isoflux condition, aluminum fins have been incorporated on the top of the alumina substrate at the hot end. To remove convective heat loss, TEGs have been considered to be placed in still transparent air.[40] The developed output voltage at one end and the ground terminal (0 V) at another end of the module have been regarded as the electrical boundary condition.

Energy Balance Equation. Considering the thermoelectric generator is in steady state, material properties are temperature-independent, and environmental heat loss is negligible, the energy balance on the cold and hot sides (shown in Figure S2(a)) can be given as

$$Q_h + {}^{Q_j}\!/_2 - Q_{ph} - Q_{TEG} = 0 \tag{1}$$

$$-Q_c + {}^{Q_j}\!/_2 + Q_{pc} + Q_{TEG} = 0 \tag{2}$$

where Q_h, Q_c, Q_j, Q_{ph}, Q_{pc}, and Q_{TEG} represent heat flow from the source, heat capture in the sink, Joule heating, Peltier effect generated cooling on the hot side, Peltier effect induced cooling on the cold side, and heat flow through the TEG, respectively. A detailed one-dimensional along with three-dimensional energy balance equation have been elaborated upon in the Supporting Information.

The internal electrical and thermal resistance of the TEG ($R_{e_{TEG}}$ and $R_{th_{TEG}}$, respectively) can be denoted as

$$R_{e_{TEG}} = N\frac{h}{a}\left(\frac{1}{\sigma_p} + \frac{1}{\sigma_n}\right) \tag{3}$$

$$R_{th_{TEG}} = \frac{h}{Na}\left(\frac{1}{k_p + k_n}\right) \tag{4}$$

where N, h, a, σ, and k represent the number of leg pairs, leg height, leg area, electrical conductivity, and thermal conductivity, respectively. The suffixes n and p are utilized to signify an n- or p-type leg, respectively.

Two dimensionless geometrical parameters connecting leg width (w) and module area (A) and known as fill fraction (FF) and aspect ratio (AR) can be defined as[32,41]

$$FF = 2N\frac{w^2}{A} \tag{5}$$

$$AR = \frac{h}{w} \tag{6}$$

Utilizing eqs 5 and 6, eq 3 can be rewritten as

$$R_{e_{TEG}} = 2N^2\frac{w \times AR}{A \times FF}\left(\frac{1}{\sigma_p} + \frac{1}{\sigma_n}\right) \tag{7}$$

Under optimal load ($R_L = R_{e_{TEG}}\sqrt{1 + Z\bar{T}}$), the load voltage ($V_{opt}$), TEG power output ($P_{opt}$), and maximum efficiency (η_{max}) can be

$$V_{opt} = NS(T_h - T_c)\frac{\sqrt{1 + Z\bar{T}}}{1 + \sqrt{1 + Z\bar{T}}} \tag{8}$$

$$P_{opt} = \frac{(NS(T_h - T_c))^2}{R_{e_{TEG}}}\frac{\sqrt{1 + Z\bar{T}}}{(1 + \sqrt{1 + Z\bar{T}})^2} \tag{9}$$

$$\eta_{\max} = \frac{P_{opt}}{Q_h} = \frac{T_h - T_c}{T_h}\left[\frac{\sqrt{1 + Z\bar{T}} - 1}{\sqrt{1 + Z\bar{T}} + \frac{T_c}{T_h}}\right] \tag{10}$$

where $\bar{T} = \frac{T_c + T_h}{2}$, $\Delta T = (T_h - T_c)$ and T_c, T_h, S, and $Z\bar{T}$ represents the cold end temperature, hot end temperature, effective Seebeck coefficient ($S = S_p - S_n$) and TEG module figure of merit at mean temperature, respectively.

Temperature-dependent properties of the TE material result in the generation of thermal stress when exposed to temperature differences. Along the direction of the temperature gradient, the generated

https://doi.org/10.1021/acsaem.1c01466
ACS Appl. Energy Mater. 2021, 4, 8211−8219

temperature field can be obtained by solving the three-dimensional thermodynamic equation

$$\frac{\partial}{\partial x}\left[k\frac{\partial T}{\partial x}\right] + \frac{\partial}{\partial y}\left[k\frac{\partial T}{\partial y}\right] + \frac{\partial}{\partial z}\left[k\frac{\partial T}{\partial z}\right] = 0 \tag{11}$$

where $k = f(T)$ and $T = f(x,y,z)$

Displacement strain due to thermal stress can be given by

$$\bar{\varepsilon}_{xx} = \frac{\partial \bar{u}}{\partial \bar{x}};\ \bar{\varepsilon}_{yy} = \frac{\partial \bar{v}}{\partial \bar{y}};\ \bar{\varepsilon}_{zz} = \frac{\partial \bar{w}}{\partial \bar{z}};\ \bar{\varepsilon}_{yx} = \frac{1}{2}\left(\frac{\partial \bar{u}}{\partial \bar{y}} + \frac{\partial \bar{v}}{\partial \bar{x}}\right);$$

$$\bar{\varepsilon}_{yz} = \frac{1}{2}\left(\frac{\partial \bar{w}}{\partial \bar{y}} + \frac{\partial \bar{v}}{\partial \bar{z}}\right);\ \bar{\varepsilon}_{xz} = \frac{1}{2}\left(\frac{\partial \bar{w}}{\partial \bar{x}} + \frac{\partial \bar{u}}{\partial \bar{z}}\right) \tag{12}$$

The stress−strain relationship can be established by using the dimensionless Jacobian matrix.[42] Further, three principal stress components (σ_1, σ_2, σ_3) have been applied to calculate the equivalent von Mises stress as given by eq 13

$$\sigma = \frac{\sqrt{(\sigma_1 - \sigma_2)^2 + (\sigma_2 - \sigma_3)^2 + (\sigma_3 - \sigma_1)^2}}{2} \tag{13}$$

RESULT AND DISCUSSION

In order to understand the effectiveness of SnSe for application in the TEG, p-type and n-type unilegs of identical dimensions (3 × 3 × 4 mm) have been subjected to a constant heat gradient of ΔT = 473 K (T_h = 773 K). As shown in Figure 2, p-type SnSe has attained a maximum conversion efficiency (η_{max}) of 14.187% at 6.0 mΩ and maximum power output ($P_{out_{max}}$) of 3.086 W at 1.0 mΩ. On the contrary, the n-type SnSe unileg has shown a much inferior performance (η_{max} = 4.907% and $P_{out_{max}}$ = 0.1116 W), which can seriously affect the overall performance of the Π-architecture TEG, where both n-type and p-type legs are used. The specific contact resistivity ($\rho_{contact}$) of p- and n-legs has been estimated by utilizing the established relationship for calculating contact resistance of unicouple TEG[5] (eq 14).

$$R = N\left(\frac{\rho_n h_n}{A_n} + \frac{\rho_p h_p}{A_p} + R_c\right) \tag{14}$$

where R, ρ, h, and A represent resistance, resistivity, length (height), and cross-sectional area of the thermoelectric leg and R_c accounts for interconnects and contact resistance. $\rho_{contact}$ has been estimated to be 62 μΩ cm^2 for the p-leg, which is much lower in comparison to the n-type (2.16 mΩ cm^2). The superior performance of the p-type SnSe has offered the possibility of designing a multiple unilegged architecture. Hence, we have modeled a multiple unilegged TEG consisting of 36 p-type SnSe legs (as shown in Figure 1(b)) by utilizing the optimized simulation parameters tabulated in Table 1. Further, we have compared the simulation results of the 36 p-type unilegged architecture with a TEG of a 36 n-p configuration. Based on the geometrical optimization of the n-leg shape (as detailed in the Supporting Information), cylindrical and coneUp4 shapes have shown the best performance under the isothermal and isoflux heat boundary conditions, respectively. So, for further study, they have been utilized in multiple p−n-leg architecture as an n-leg shape along with square p-legs.

Under the Isothermal Heat Boundary. The performances of modeled multiple p-legged and Π-architecture have been studied in a COMSOL Multiphysics simulation by utilizing the optimized simulation parameters tabulated in Table 1 under the isothermal heat boundary condition. In our model, we have considered both ideal situation, i.e., without any loss and a practical case where the electrical contact loss along with conductive and radiative heat losses have been incorporated. Figure 3(a) demonstrates the power output of multiple p-legged and p−n-legged TEGs under a working load (0.5−5 Ω). A multiple p-legged TEG has shown a $P_{out_{max}}$ of 21.39 W under ideal conditions and 6.61 W after cogitating the losses at 0.5 Ω. Whereas, Π-architecture has exhibited a $P_{out_{max}}$ of 6.06 W at 0.5 Ω under the ideal situation, which further drops to 2.64 W at 1.5 Ω while considering the losses. The variation of output voltage and current with load resistance for the multiple p-legged and p−n-legged architecture considering losses are displayed in Figure S4. The leading cause behind such significant variation in power output is the relatively smaller value of $R_{e_{TEG}}$ and specific contact resistivity of the multiple p-legged architecture.

Figure 3(b) reveals that the maximum efficiency (η_{max}) of multiple p−n-legged architecture is 16.27% under the ideal condition, which is relatively higher than the multiple p-legged architecture (10.47%), contradicting the expected trend. After all the losses have been considered, a maximum efficiency of 4.8% has been achieved for Π-architecture, whereas multiple p-legged geometry has resulted in η_{max} = 3.48%. The divergence in the result is mainly caused by the change in geometry of the n-leg as the rate of heat transfer inherently depends on leg geometry.[43]

Under the Isoflux Heat Boundary. Similar work has been further carried out under the isoflux (constant heat rate) heat boundary condition as most of the real-world applications, especially automobile exhaust, impart heat at a constant rate. A p−n-multilegged TEG module having an optimized cone-up4 n-leg has been put under a constant input flux (h_f) of 10^4 W/m^2 while maintaining the same simulation parameters as the isothermal condition. A very poor performance of the TEG ($P_{out_{max}} \approx 0.34$ W and $\eta_{max} \approx 1.17\%$), as shown in Figure S5(a), has compelled us to explore system level optimization by enhancing the heat capturing area. One of the easiest ways of expanding the heat receiving end is to increase the ceramic plate dimension. It has been shown in Figure S6(a) that for a

Table 1. Important Geometric and Simulation Parameters Utilized to Analyze the Performance of the TEG

parameter description	
leg length	4 mm
leg base area	3 × 3 mm
module area	54 × 54 mm
fill fraction	11%
aspect ratio	1.33
electrode and connector material	Pt
electrode and connector thickness	1 mm
substrate material	Al_2O_3
hot side temperature	773 K
hot side input heat flux	10^4 W/m^2
cold side temperature	300 K
ambient temperature	300 K
radiation emissivity for leg surface	0.45
p-leg specific contact resistivity	62 μΩ cm^2
n-leg specific contact resistivity	2.16 mΩ cm^2
working load	0.5−5 Ω

https://doi.org/10.1021/acsaem.1c01466
ACS Appl. Energy Mater. 2021, 4, 8211−8219

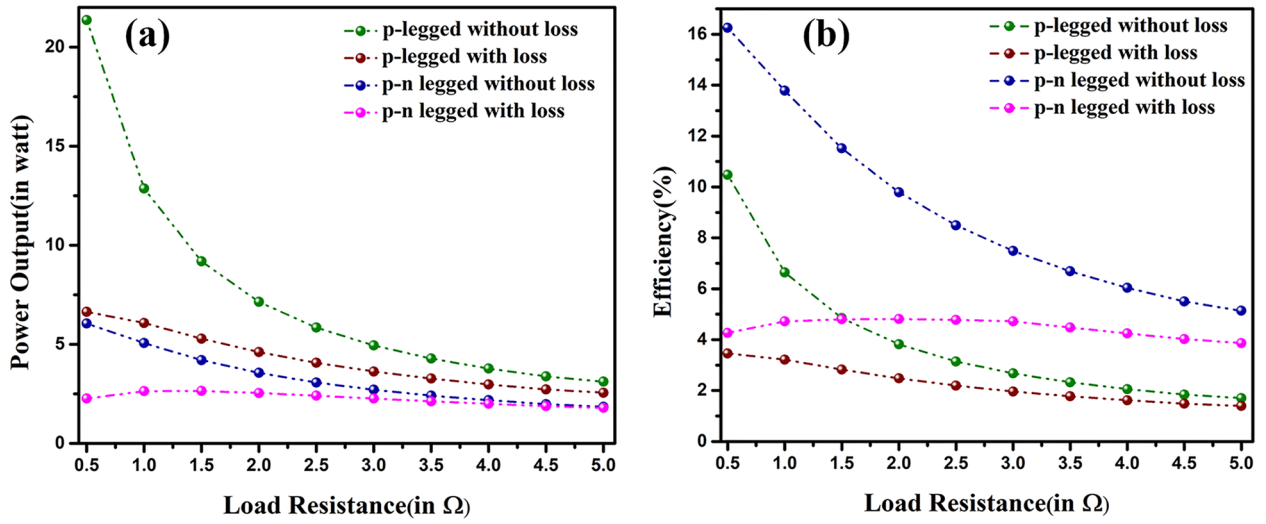

Figure 3. (a) Power output and (b) efficiency vs load resistance under the isothermal heat boundary condition.

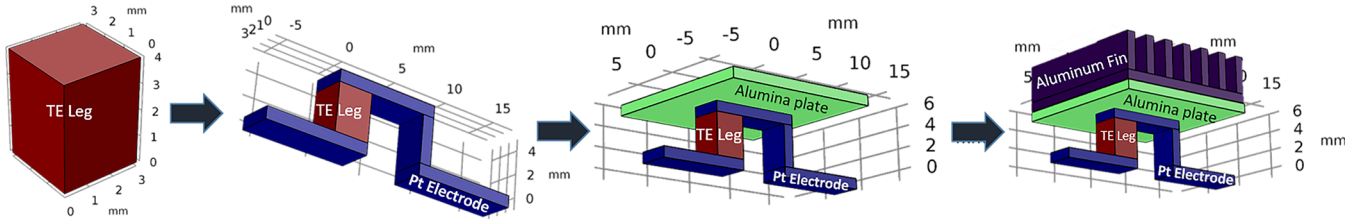

Figure 4. Various procedures implemented for enhancing the unileg performance. The figure shows a thermoelectric leg, a unileg with Pt electrodes, the introduction of an alumina plate, and the introduction of aluminum fins as heat collectors.

unicouple architecture, an increase in the size of an alumina plate (12 × 12 and 16 × 16 mm) successively has enhanced the power output. But the restriction arises as the ceramic plate cannot be enlarged ad infinitum due to the small exhaust diameter. In order to overcome that, the concept of a fin has been introduced into the present work. An aluminum fin of a thickness of 1 mm and height of 4 mm (a stepwise process shown in Figure 4) has been incorporated on the top of the ceramic plate at the hot end. The performance enhancement in the unileg TEG has been studied for five and seven fins, as shown in Figure S6. Even with a smaller plate area, an increase in the number of fins has enhanced the maximum temperature attained at the hot end (Figure S6(c)), which has further improved maximum power output and efficiency. In order to validate this argument of performance improvement in terms of power output, we have compared two architectures having the same net heat capturing area, i.e., one having 10 fins (Figure S5(b)) and another one having a hot plate with the same effective area (Figure S5(c)), keeping all other geometrical parameters unchanged as mentioned in Table 1. It has been revealed that the maximum power of 10.7 W has been obtained for both of the conditions at the same sweeping resistance of 2.6 Ω (Figure S5(d)). This result has indicated that $R_{e_{TEG}}$ is same for both configurations and, hence, the same *FF* (eqs 5 and 7). Employing this contention fill fraction under the isoflux condition can be redefined as

$$FF_{iso} = 2N\frac{w^2}{A_h} \tag{15}$$

where FF_{iso} and A_h represent the fill fraction under the isoflux condition and net heat capturing area, respectively. This analysis has posited an easier way to alter the *FF* of the TEG under the isoflux condition without tampering with the internal parameters.

By utilizing the similar argument of fin incorporation, the heat capturing area of a multiple p-legged module can also be enhanced. An increase in fin height from 4 to 20 mm has shown a change in *FF* from ∼11 to ∼1.5% ($FF_{11\%}$, $FF_{5.2\%}$, $FF_{2.3\%}$, and $FF_{1.5\%}$ respectively for no fin and fin heights of 4, 12, and 20 mm) without any alteration of aspect ratio. Figure 5(a,b) demonstrates the performance of the TEG under an ideal scenario without taking into account of any loss; whereas Figure 5(c,d) showcases the thermoelectric performances when losses are included under the isoflux heat boundary condition. It is evident from Figure 5 that even without altering the aspect ratio, improvement of *FF* can integrally enhance the performance of the TEG under the isoflux condition. The limit of reduction of *FF* has been controlled by the attained maximum temperature of SnSe legs (as shown in Figure 5(e,f)) to prevent any thermal damage (SnSe melting point: 1133 K[44]). Temperature distribution across the TEG for all the other *FF*s has been demonstrated in Figure S7. Under the ideal condition (Figure 5(a)), the multiple p-legged TEG with an *FF* ≈ 1.5% has revealed the best power output ($P_{out_{max}}$) of 10.654 W. Whereas, its p−n counterpart having an *FF* ≈ 5.2% has shown $P_{out_{max}}$ = 9.6 W. Considering a practical situation, where thermal and electrical losses have been counted, a multiple p-legged architecture with *FF* ≈ 1.5% has displayed almost 500% enhancement in power output ($P_{out_{max}}$ = 3.45 W) compared to its Π counterpart ($P_{out_{max}}$ = 0.56 W) as shown in Figure 5(c). The variation of current and voltage with load resistance for a

https://doi.org/10.1021/acsaem.1c01466
ACS Appl. Energy Mater. 2021, 4, 8211−8219

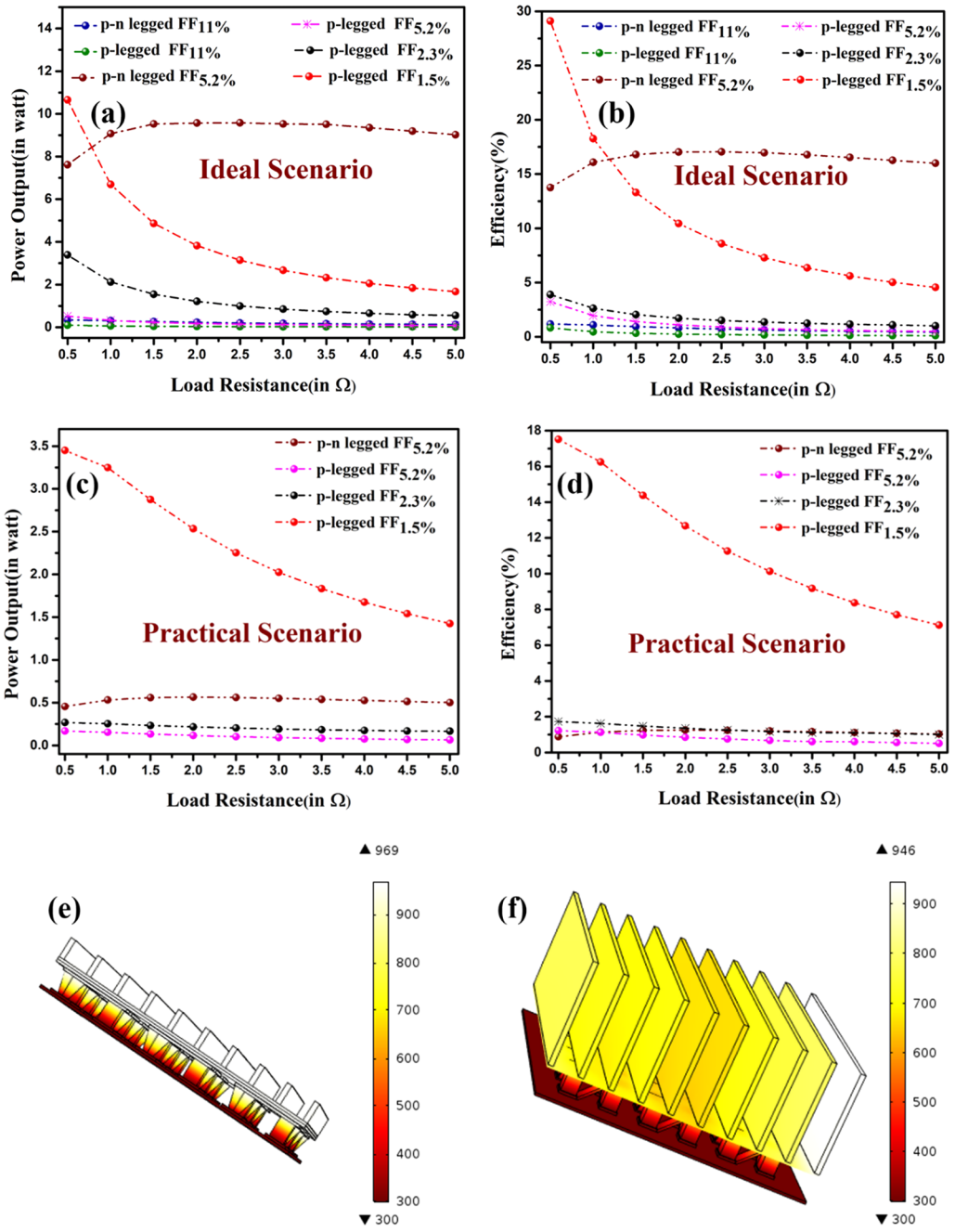

Figure 5. Variation of (a) power output and (b) efficiency with load resistance considering the ideal condition without any loss. The plots of (c) power output vs load resistance and (d) efficiency vs load resistance after considering electrical and thermal losses under the isoflux heat boundary condition. Temperature distribution in an optimized TEG with (e) Π architecture and (f) p-legged architecture.

multiple p-legged structure with $FF \approx 1.5\%$ and multiple p−n-legged structure having $FF \approx 5.2\%$ considering all the losses is shown in Figure S8. It is well-known that efficiency of the TEG depends on both the power output and the heat flow from the source. Under the isoflux heat boundary condition, heat flows from source at a constant rate, and hence, it is expected that system having the best power output will show the best efficiency (as indicated in Figure 5(b,d)), which may not be true for the isothermal condition. As shown in Figure 5(b), under the ideal condition, a maximum efficiency (η_{max}) of 29.11% has been achieved by a multiple p-legged structure with $FF \approx 1.5\%$, and $\eta_{max} = 17\%$ has been accomplished by a Π architecture having $FF \approx 5.2\%$. Interestingly, under the real-world scenario considering thermal and electrical losses, the multiple p-legged architecture with *FF* app 1.5% has resulted in $\eta_{max} = 17.5\%$, which is almost 14 times higher than the Π architecture having $FF \approx 5.2\%$ ($\eta_{max} = 1.24\%$). Because the practical application is very close to the isoflux heat source condition taking into account various heat losses and electrical contact loss, it can be concluded that order of magnitude increase in the performance of the TEG can be realized by adopting the multiple p-legged architecture instead of the traditional Π architecture.

Thermal Stress Analysis. The thermoelectric performance and lifetime of the TEG rely on the thermomechanical functioning of the module. In order to understand the effect of

https://doi.org/10.1021/acsaem.1c01466
ACS Appl. Energy Mater. 2021, 4, 8211−8219

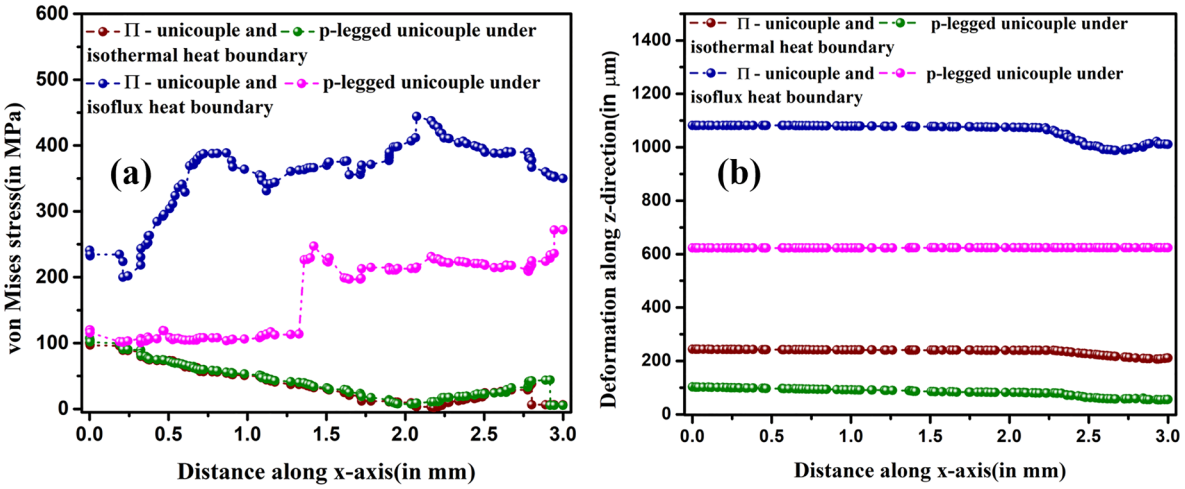

Figure 6. (a) von Mises stress developed and (b) deformation along the direction of heat flow at the critical junction under the isothermal and isoflux heat boundary conditions.

larger ΔT as well as the high input heat flux on the optimized TEG module for the isothermal as well as isoflux conditions respectively, von Mises stress generation and effective deformation due to generated stress have been studied. Table S1 represents the necessary properties of SnSe used in thermal stress analysis. Since our point of interest is to understand the deformation and stress at the junction of different materials, we have considered the junction point of the TE leg, electrode, and ceramic plate for the study. A simplified two -leg model (Π-unicouple and p-legged unicouple) has been considered. Generated von Mises stress in the modules under the isothermal condition is shown in Figure S9(a,b). A similar analysis has been performed while considering a two-legged section of the best performing architecture (Π-architecture having $FF \approx 5.2\%$ and multiple p-legged having $FF \approx 1.5\%$) under the isoflux heat boundary condition. The produced von Mises stress is presented in Figure S9(c,d). An in-depth analysis of generated stress and deformation on the junction region has been further executed under both of the heat boundary conditions as presented in Figure 6. It is evident from Figure 6(a) that the generated von Misses stress on the Π-unicouple is much higher compared to its p-legged counterpart, especially under the isoflux heat boundary condition. The primary reasons behind such a phenomenon are attributed the presence of the n-leg having different thermoelectric properties and the coefficient of thermal expansion, besides the higher maximum temperature attained by the junction of our study, as shown in Figure 5(e,f). The presence of a greater number of materials (additional aluminum fin) with a different thermal expansion coefficient (CTE) at the junction region might have contributed to the stress generation. Under the isothermal heat boundary condition, because the maximum temperatures attained for both the Π-unicouple and p-legged unicouple are identical (773 K), similar von Misses stress was found for both of the architectures. Deformation along the direction of heat flow with the varying leg width (as shown in Figure 6(b)) implies that lesser deformation has occurred in multiple p-legged modules under both isothermal and isoflux heat boundary conditions. Thus, the analysis of both isothermal and isoflux conditions has indicated that the multiple p-legged module is less prone to structural deformation at the critical junctions even in the presence of a higher degree of generated von Mises stress (~MPa), making it structurally and mechanically more reliable.

CONCLUSION

In summary, we have performed finite element modeling of a SnSe-based TEG with two different architectures, namely, multiple p-legged and p−n-legged (Π) modules under the isothermal heat boundary condition as well as the isoflux heat boundary condition, which is generally found in practical applications like automotive exhaust. Under the isothermal heat boundary condition, a maximum power output of 6.61 W has been achieved for the multiple p-legged TEG, which is ~2.5 times greater than that obtained for the multiple p−n-legged module considering all the losses. Interestingly, the maximum efficiency of 4.8% obtained in the Π-module is found to be slightly higher than the multiple p-legged architecture. For the isoflux heat boundary, we have seen the heat capturing area has played a crucial role in the TEG performance. In order to enhance heat capturing area to improve output power and efficiency, fin of different heights (4, 12, and 20 mm) have been incorporated at the hot end for both multiple p-legged and p−n-legged structures. In this context, we have redefined the concept of fill fraction (FF) by incorporating heat capturing area for easier optimization without manipulating internal parameters. Under the isoflux heat boundary condition, incorporation of a fin has resulted in a maximum power output of 3.45 W and efficiency of 17.5% for a multiple p-legged architecture having $FF \approx 1.5\%$, which is significantly higher than the best performing p−n architecture ($P_{out_{max}} = 0.56$ W and $\eta_{max} = 1.24\%$) while considering all the losses. Thermal analysis for mechanical and structural stability has shown that the the proposed multiple p-legged structure is more stable and prone to lesser deformation even under high input heat flux. The overall performance analysis has indicated that multiple p-legged TEG with Al fins at the hot end resulting in a low fill fraction (~1.5) is a suitable architecture of the TEG for waste-heat recovery from automotive exhaust.

ASSOCIATED CONTENT

Supporting Information

The Supporting Information is available free of charge at https://pubs.acs.org/doi/10.1021/acsaem.1c01466.

https://doi.org/10.1021/acsaem.1c01466
ACS Appl. Energy Mater. 2021, 4, 8211−8219

Thermoelectric properties of SnSe, three-dimensional energy balance equation, detailed one-dimensional energy balance equation, optimization of the TEG leg shape, change in current and voltage with load resistance for multiple p-legged architecture and multiple p−n-legged architecture under the isothermal condition considering all the losses, performance of multiple p−n-legged TEG in the absence of a fin and concept of equivalent heat capturing area, power output vs load plot while increasing heat capturing area, temperature distribution for *FF* = 11% for multiple p−n-legged architecture and *FF* = 11, 5.2, and 2.3% for multiple p-legged module under the isoflux heat boundary, change in current and voltage with load resistance for multiple p-legged architecture and multiple p−n-legged architecture under the isoflux condition considering all the losses, comprehensive table on material properties used for thermal analysis, von Mises stress diagram under the isothermal and isoflux heat boundary conditions (PDF)

AUTHOR INFORMATION

Corresponding Author

Tanmoy Maiti − *Plasmonics and Perovskites Laboratory, Department of Materials Science and Engineering, IIT Kanpur, Kanpur, U.P. 208016, India;* orcid.org/0000-0003-1581-7614; Phone: +91-512-259-6599; Email: tmaiti@iitk.ac.in

Authors

Monikuntala Bhattacharya − *Plasmonics and Perovskites Laboratory, Department of Materials Science and Engineering, IIT Kanpur, Kanpur, U.P. 208016, India*

Mani Ranjan − *Plasmonics and Perovskites Laboratory, Department of Materials Science and Engineering, IIT Kanpur, Kanpur, U.P. 208016, India*

Nitish Kumar − *U R Rao Satellite Centre, Indian Space Research Organization, Bengaluru 560017, India*

Complete contact information is available at: https://pubs.acs.org/10.1021/acsaem.1c01466

Notes

The authors declare no competing financial interest.

ACKNOWLEDGMENTS

The authors acknowledge the financial support from the Indian Space Research Organization (ISRO) under Grant STC/MET/2018112.

REFERENCES

(1) Forman, C.; Muritala, I. K.; Pardemann, R.; Meyer, B. Estimating the global waste heat potential. *Renewable Sustainable Energy Rev.* **2016**, *57*, 1568−1579.

(2) Merkisz, J.; Fuc, P.; Lijewski, P.; Ziolkowski, A. Waste energy recovery analysis of a diesel engine exhaust system. *WIT Trans. Eng. Sci.* **2014**, *83*, 93.

(3) Sivaprahasam, D.; Harish, S.; Gopalan, R.; Sundararajan, G. Automotive Waste Heat Recovery by Thermoelectric Generator Technology. *Bringing Thermoelectricity into Reality* **2018**. DOI: 10.5772/intechopen.75443

(4) Gou, X.; Xiao, H.; Yang, S. Modeling, experimental study and optimization on low-temperature waste heat thermoelectric generator system. *Appl. Energy* **2010**, *87* (10), 3131−3136.

(5) Aswal, D. K.; Basu, R.; Singh, A. Key issues in development of thermoelectric power generators: High figure of merit materials and their highly conducting interfaces with metallic interconnects. *Energy Convers. Manage.* **2016**, *114*, 50−67.

(6) Zhao, Q.; Qin, B.; Wang, D.; Qiu, Y.; Zhao, L.-D. Realizing high thermoelectric performance in polycrystalline SnSe via silver doping and germanium alloying. *ACS Applied Energy Materials* **2020**, *3* (3), 2049−2054.

(7) Hasan, M. N.; Wahid, H.; Nayan, N.; Mohamed Ali, M. S. Inorganic thermoelectric materials: A review. *Int. J. Energy Res.* **2020**, *44* (8), 6170−6222.

(8) Wang, H.; McCarty, R.; Salvador, J. R.; Yamamoto, A.; König, J. Determination of thermoelectric module efficiency: A survey. *J. Electron. Mater.* **2014**, *43* (6), 2274−2286.

(9) Chen, Y.; Wang, X.; Li, D.; Hong, R.; Shen, H. Parameters extraction from commercial solar cells I-V characteristics and shunt analysis. *Appl. Energy* **2011**, *88* (6), 2239−2244.

(10) Deppe, T.; Munday, J. N. Nighttime Photovoltaic Cells: Electrical Power Generation by Optically Coupling with Deep Space. *ACS Photonics* **2020**, *7* (1), 1−9.

(11) Yazawa, K.; Shakouri, A. Optimization of power and efficiency of thermoelectric devices with asymmetric thermal contacts. *J. Appl. Phys.* **2012**, *111* (2), 024509.

(12) Mayer, P.; Ram, R. Optimization of heat sink-limited thermoelectric generators. *Nanoscale Microscale Thermophys. Eng.* **2006**, *10* (2), 143−155.

(13) Chen, L.; Gong, J.; Sun, F.; Wu, C. Effect of heat transfer on the performance of thermoelectric generators. *Int. J. Therm. Sci.* **2002**, *41* (1), 95−99.

(14) Kishore, R. A.; Mahajan, R. L.; Priya, S. Combinatory finite element and artificial neural network model for predicting performance of thermoelectric generator. *Energies* **2018**, *11* (9), 2216.

(15) Wei, T.-R.; Wu, C.-F.; Zhang, X.; Tan, Q.; Sun, L.; Pan, Y.; Li, J.-F. Thermoelectric transport properties of pristine and Na-doped SnSe 1- x Te x polycrystals. *Phys. Chem. Chem. Phys.* **2015**, *17* (44), 30102−30109.

(16) Dunham, M. T.; Barako, M. T.; LeBlanc, S.; Asheghi, M.; Chen, B.; Goodson, K. E. Power density optimization for micro thermoelectric generators. *Energy* **2015**, *93*, 2006−2017.

(17) Yang, R.; Chen, G.; Snyder, G. J.; Fleurial, J.-P. Multistage thermoelectric microcoolers. *J. Appl. Phys.* **2004**, *95* (12), 8226−8232.

(18) Sahin, A. Z.; Yilbas, B. S. The thermoelement as thermoelectric power generator: effect of leg geometry on the efficiency and power generation. *Energy Convers. Manage.* **2013**, *65*, 26−32.

(19) Stobart, R.; Yang, Z.; Lan, S. System design considerations for thermoelectric energy recovery. *Thermoelectric Materials and Devices* **2016**, *17*, 156−203.

(20) Crane, D. T.; Jackson, G. S. Systems-level optimization of low-temperature thermoelectric waste heat recovery. *2002 37th Intersociety Energy Conversion Engineering Conference (IECEC)* **2004**, 583−591.

(21) Bilotti, E.; Fenwick, O.; Schroeder, B. C.; Baxendale, M.; Taroni-Junior, P.; Degousée, T.; Liu, Z. Organic Thermoelectric Composites Materials. *In Comprehensive Composite Materials II* **2018**, *6*, 408−430.

(22) Chen, M.; Rosendahl, L. A.; Condra, T. A three-dimensional numerical model of thermoelectric generators in fluid power systems. *Int. J. Heat Mass Transfer* **2011**, *54* (1−3), 345−355.

(23) Korotkov, A.; Loboda, V.; Makarov, S.; Feldhoff, A. Modeling thermoelectric generators using the ANSYS software platform: Methodology, practical applications, and prospects. *Russ. Microelectron.* **2017**, *46* (2), 131−138.

(24) Wu, Y.; Ming, T.; Li, X.; Pan, T.; Peng, K.; Luo, X. Numerical simulations on the temperature gradient and thermal stress of a thermoelectric power generator. *Energy Convers. Manage.* **2014**, *88*, 915−927.

(25) Erturun, U.; Mossi, K. A feasibility investigation on improving structural integrity of thermoelectric modules with varying geometry. *ASME 2012 Conference on Smart Materials, Adaptive Structures and Intelligent Systems* **2012**, 939−945.

(26) Hori, Y.; Kusano, D.; Ito, T.; Izumi, K. Analysis on thermo-mechanical stress of thermoelectric module. *Eighteenth International Conference on Thermoelectrics. Proceedings, ICT'99* **1999**, 328−331.
(27) Nakatani, Y.; Shindo, T.; Wakamatsu, K.; Hino, T.; Ohishi, T.; Matsumuro, H.; Itoh, Y. Evaluation on Thermo-Mechanical Integrity of Thermoelectric Module for Heat Recovery at Low Temperature. *Developments in Strategic Materials: Ceramic Engineering and Science Proceedings* **2008**, *29* (10), 69−76.
(28) Li, S.-L.; Liu, C.-K.; Hsu, C.-Y.; Hsieh, M.-C.; Dai, M.-J.; Wu, S.-T. Thermo-mechanical analysis of thermoelectric modules. *2010 5th International Microsystems, Packaging, Assembly and Circuits Technology Conference (IMPACT)* **2010**, 1−4.
(29) Nemoto, T.; Iida, T.; Sato, J.; Sakamoto, T.; Nakajima, T.; Takanashi, Y. Power generation characteristics of Mg 2 Si uni-leg thermoelectric generator. *J. Electron. Mater.* **2012**, *41* (6), 1312−1316.
(30) Nemoto, T.; Iida, T.; Sato, J.; Sakamoto, T.; Hirayama, N.; Nakajima, T.; Takanashi, Y. Development of an Mg 2 Si unileg thermoelectric module using durable Sb-doped Mg 2 Si legs. *J. Electron. Mater.* **2013**, *42* (7), 2192−2197.
(31) Wang, X.; Wang, H.; Su, W.; Zhai, J.; Wang, T.; Chen, T.; Mehmood, F.; Wang, C. Optimization of the performance of the SnTe uni-leg thermoelectric module via metallized layers. *Renewable Energy* **2019**, *131*, 606−616.
(32) Kishore, R. A.; Nozariasbmarz, A.; Poudel, B.; Priya, S. High-Performance Thermoelectric Generators for Field Deployments. *ACS Appl. Mater. Interfaces* **2020**, *12* (9), 10389−10401.
(33) Ranjan, M.; Maiti, T. Device Modeling and Performance Optimization of Thermoelectric Generators under Isothermal and Isoflux Heat Source Condition. *J. Power Sources* **2020**, *480*, 228867.
(34) Espinosa, N.; Lazard, M.; Aixala, L.; Scherrer, H. Modeling a thermoelectric generator applied to diesel automotive heat recovery. *J. Electron. Mater.* **2010**, *39* (9), 1446−1455.
(35) Zhao, L.-D.; Lo, S.-H.; Zhang, Y.; Sun, H.; Tan, G.; Uher, C.; Wolverton, C.; Dravid, V. P.; Kanatzidis, M. G. Ultralow thermal conductivity and high thermoelectric figure of merit in SnSe crystals. *Nature* **2014**, *508* (7496), 373−377.
(36) Chang, C.; Wu, M.; He, D.; Pei, Y.; Wu, C.-F.; Wu, X.; Yu, H.; Zhu, F.; Wang, K.; Chen, Y.; et al. 3D charge and 2D phonon transports leading to high out-of-plane ZT in n-type SnSe crystals. *Science* **2018**, *360* (6390), 778−783.
(37) Gainza, J.; Serrano-Sánchez, F.; Rodrigues, J. E.; Huttel, Y.; Dura, O. J.; Koza, M. M.; Fernández-Díaz, M. T.; Meléndez, J. J.; Márkus, B. G.; Simon, F.; et al. High-Performance n-type SnSe Thermoelectric Polycrystal Prepared by Arc-Melting. *Cell Reports Physical Science* **2020**, *1* (12), 100263.
(38) Zhao, L.-D.; Tan, G.; Hao, S.; He, J.; Pei, Y.; Chi, H.; Wang, H.; Gong, S.; Xu, H.; Dravid, V. P.; et al. Ultrahigh power factor and thermoelectric performance in hole-doped single-crystal SnSe. *Science* **2016**, *351* (6269), 141−144.
(39) Alkidas, A. C.; Battiston, P. A.; Kapparos, D. J. Thermal Studies in the Exhaust System of a Diesel-Powered Light-Duty Vehicle. *SAE Tech. Pap. Ser.* **2004**, 2004-01-0050.
(40) Bjørk, R.; Christensen, D. V.; Eriksen, D.; Pryds, N. Analysis of the internal heat losses in a thermoelectric generator. *Int. J. Therm. Sci.* **2014**, *85*, 12−20.
(41) Nozariasbmarz, A.; Kishore, R. A.; Poudel, B.; Saparamadu, U.; Li, W.; Cruz, R.; Priya, S. High Power Density Body Heat Energy Harvesting. *ACS Appl. Mater. Interfaces* **2019**, *11* (43), 40107−40113.
(42) Shittu, S.; Li, G.; Zhao, X.; Ma, X.; Akhlaghi, Y. G.; Ayodele, E. Optimized high performance thermoelectric generator with combined segmented and asymmetrical legs under pulsed heat input power. *J. Power Sources* **2019**, *428*, 53−66.
(43) Ali, H.; Sahin, A. Z.; Yilbas, B. S. Thermodynamic analysis of a thermoelectric power generator in relation to geometric configuration device pins. *Energy Convers. Manage.* **2014**, *78*, 634−640.
(44) Agarwal, A.; Chaki, S. H.; Lakshminarayana, D. Growth and thermal studies of SnSe single crystals. *Mater. Lett.* **2007**, *61* (30), 5188−5190.

https://doi.org/10.1021/acsaem.1c01466
ACS Appl. Energy Mater. 2021, 4, 8211−8219